COMMUNICATIONS CHEMISTRY

ARTICLE

OPEN

Accumulation of persistent tungsten in bone as in situ generated polytungstate

Cassidy R. VanderSchee [1], David Kuter [1,2], Alicia M. Bolt[3], Feng-Chun Lo[4], Renfei Feng[5], Juergen Thieme[6], Yu-chen Karen Chen-Wiegart[6], Garth Williams[6], Koren K. Mann[3] & D. Scott Bohle[1]

Tungsten accumulates in bone but is neither labile nor inert once absorbed. Tungsten's relatively high cytosolic solubility and availability are problematic given its association with childhood lymphocytic leukemia. In light of tungsten's technological prevalence, and the increased concern of regulatory agencies, here we characterize the chemical form and localization in mice exposed to tungsten through drinking water. Using X-ray fluorescence spectroscopy, we report accumulation of tungsten in bone tissue with some sites having ~10-fold greater intensities than background levels. The long bone tissue studied includes cortical, cancellous and bone marrow. Persistence of tungsten in cortical bone tissue following removal of the source indicates that it is retained in an insoluble form. The X-ray absorption near-edge structure spectra for tungsten in these tissues indicate that it is no longer in the originally administered form, orthotungstate, but rather resembles the heteropolytungsate species, phosphotungstate.

[1] Department of Chemistry, McGill University, Montreal, H3A0B8, Canada. [2] Department of Chemistry and Polymer Science, Stellenbosch University, Private Bag X1, Stellenbosch, 7602, South Africa. [3] Lady Davis Institute for Medical Research, McGill University, 3755 Cote Ste Catherine Rd, Montreal, H3T 1E2, Canada. [4] Department of Chemistry, National Tsing Hua University, Hsinchu, 30013, Taiwan. [5] Canadian Light Source Inc, 44 Innovation Boulevard Saskatoon, Saskatoon, SK S7N 2V3, Canada. [6] Brookhaven National Laboratory, 743 Brookhaven Avenue, Building 743, Upton, NY 11973-5000, USA. Correspondence and requests for materials should be addressed to D.S.B. (email: scott.bohle@mcgill.ca)

Tungsten is the only third row transition metal with a recognized natural bioinorganic chemistry[1]. The prevalent belief that it is innocuous, coupled with its many unique properties, has led to the pervasive adoption of tungsten in a surprising range of technologies[2,3]. However, the recent association of a cluster of acute childhood lymphocytic leukemia cases in Fallon, Nevada, with elevated levels of tungsten in the community's ground water[4] has led to a reappraisal of its potential toxicity. As there remains a lack of toxicological data, tungsten was nominated as an emerging contaminant for further investigation by the US Environmental Protection Agency and National Toxicity Program.[4]

When mice ingest solubilized tungsten in the form of ortho-tungstate (WO_4^{2-}), it rapidly accumulates in their bones[5]. Other bone-accumulating metals, such as lead and strontium[6], substitute for calcium in hydroxyapatite, the calcium-phosphate matrix of bone, and can be removed using standard chelation therapy[7]. This treatment, however, is ineffective at removing anionic oxometallate anions of tungsten, which is thus retained in cortical bone tissue even after the source is removed[3,8]. This suggests alternate speciation or accumulation mechanisms for tungsten compared to other metals. To both understand the biological implications of accumulation and develop an effective treatment strategy, it is essential to determine if there is selective deposition in particular regions of bone tissue, as well as to establish the chemical form therein. Tungsten deposition may have a variety of detrimental consequences, specific to the type of bone tissue in which it is present.

Here we use synchrotron radiation micro X-ray fluorescence (SR-µXRF) spectroscopy and micro X-ray absorption near-edge structure (SR-µXANES) spectroscopy to show that tungsten is heterogeneously distributed in bone tissue and that the in vivo speciation of tungsten is in the form of in situ generated polytungstes.

Results

Distribution of tungsten in bone tissue. SR-µXRF is a non-destructive technique that has been applied in diverse fields including archeology, forensics, anthropology, and geology to simultaneously identify and spatially resolve multiple trace elements ranging from the macroscopic to microscopic scale[6]. While this technique has successfully been applied to probe the accumulation of several heavy metals in bone, it has not been used to determine the spatial distribution of bone-accumulated tungsten. The localized distribution of tungsten throughout all the main components of long bone tissue (cancellous, cortical and bone marrow) for mice exposed to 1000 ppm tungsten via sodium tungstate (Na_2WO_4) in drinking water over the course of 1, 4, and 12 weeks was thus determined using SR-µXRF. The spectra obtained were deconvoluted to visualize elemental distribution in each of the scanned XRF images.

With this technique, we observe localized, concentrated regions of tungsten in all of the main components of bone tissue (Fig. 1). These results were consistent along the length of both long bones, tibia and femur, and across all exposure times (Supplementary Fig. 1). Tungsten was found in the marrow and cancellous tissue at the end of long bone, with intensities ~10-fold higher than background levels (Fig. 1c, Supplementary Table 1). These tissues are the site of essential bone functions, such as growth and immune cell formation. Whether tungsten interferes in these processes is under investigation, however, studies have shown that mice exposed to tungsten have increased DNA damage in both whole marrow and isolated B lymphocytes, a type of white blood cell[8]. Tungsten is also incorporated into cortical bone tissue (Figs. 1d, e, and 2), which may affect bone structure and integrity.
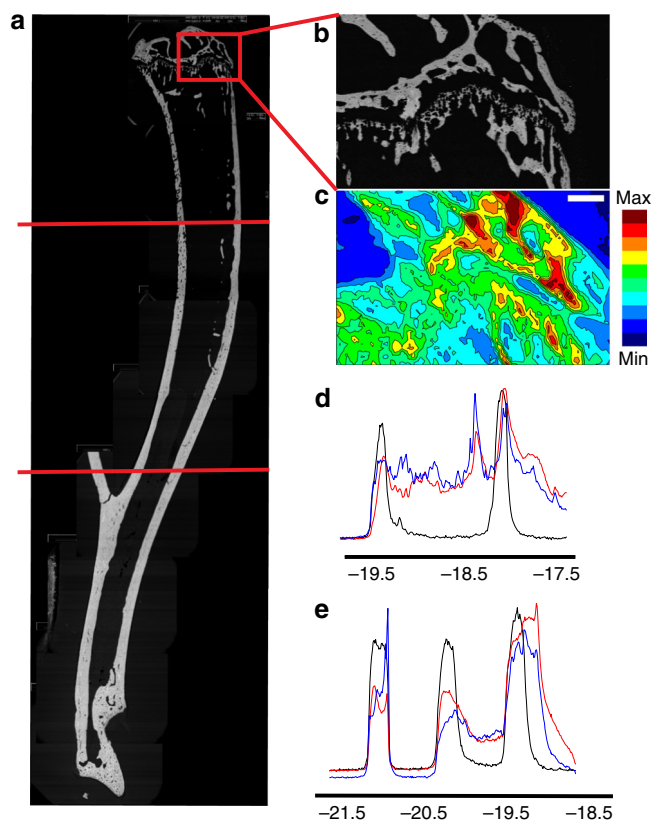
Fig. 1 Tungsten heterogeneous distribution throughout mouse tibia. **a** Backscattered electron image (BEI) of mouse tibia after 4 weeks of exposure to 1000 ppm tungsten via Na_2WO_4 in drinking water. The BEI indicates the presence of dense, calcium-containing cortical and cancellous matrix but does not display lighter organic cartilage and bone marrow. **b** BEI expansion of tibia head. **c** SR-µXRF map of tungsten distribution in area indicated in (**b**), scale bar 200 µm. **d**, **e** SR-µXRF linescans of the upper and lower lines marked in (**a**), respectively (calcium: black, tungsten: red, zinc: blue). Areas with calcium content correspond to cortical bone. X-axis is position (mm) and y-axis relative X-ray fluorescence intensity for each element. See Supplementary Table 1 for intensity values

Higher concentrations within cortical tissue compared to bone marrow indicate a mechanism of incorporation working against the concentration gradient of tungsten in blood.

The heterogeneity of tungsten deposition, particularly evident in cortical bone tissue (Fig. 2a, b), has important implications for the mechanism of uptake. This localization is particularly evident when comparing the calcium (Fig. 2a, b) and tungsten (Fig. 2c, d) distributions of a tibia shaft cross-section after 4 weeks of tungsten exposure (bone marrow removed). Calcium displays a relatively uniform distribution, which arises due to the prominent distribution of calcium in hydroxyapatite[6]. However, while calcium and most other trace elements detected with SR-µXRF display uniform distribution (Supplementary Fig. 2), tungsten's unique localized deposition suggests that tungsten is incorporated during bone growth and remodeling. This hypothesis is supported by the negligible tungsten uptake in older mice, where bone remodeling due to growth is substantially reduced[7]. The similar heterogeneity of zinc provides further support (Fig. 2e, f)[6]. Zinc is an excellent marker for bone growth and remodeling as it is known to deposit between zones of bone calcification[6,9]. The heterogeneous accumulation of both tungsten and zinc at the inner and outer edges of the cortical bone tissue is likely
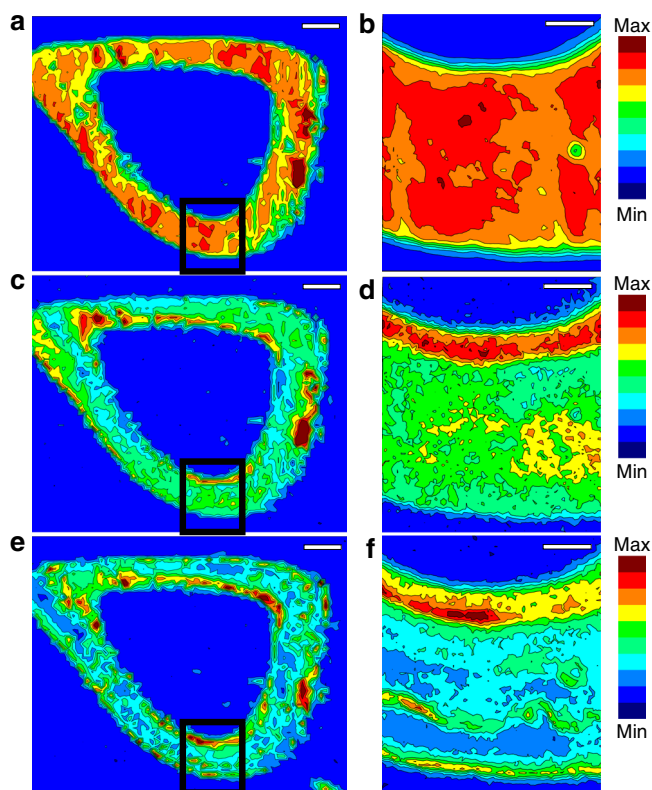
Fig. 2 Comparative maps of elemental distribution in mouse tibia cross-section. SR-µXRF images collected simultaneously of mouse tibia after 4 weeks of exposure to tungsten (1000 ppm): (**a**, **b**) calcium, (**c**, **d**) tungsten, (**e**, **f**) zinc. (**a**, **c**, **e**) Cross-sections of shaft with bone marrow removed from interior (20 µm step size). Scale bars 200 µm (**b**, **d**, **f**). Magnification of square indicated in (**a**, **c**, **e**), respectively (10 µm step size). Scale bars 50 µm. See Supplementary Table 1 for intensity values

connected to the changing width, and thus increased remodeling activity, of the long bone in these young, growing mice.

Retention of tungsten in bone tissue. Further retention experiments solidified the connection of tungsten uptake to bone remodeling. After an exposure regimen of 4 weeks of 1000 ppm tungsten (Na_2WO_4), followed by 8 weeks of tap water, tungsten deposition was mapped throughout mouse bone. Similar to the findings reported for the tibia above, tungsten was found throughout the outer cortical shell, inner cancellous tissue and bone marrow of the femur (Fig. 3a–c) after 4 weeks of exposure. However, after the source was removed, tungsten remained only in the outer cortical shell and was not detectable in the cancellous tissue or bone marrow (Fig. 3d–f). This is especially evident in the SR-µXRF overlay plots where tungsten (green) is present both in the calcium (red) containing cancellous bone tissue and in the bone marrow following 4 weeks of exposure (Fig. 3c), but no overlap is observed in this region when mice are given tungsten-free water for a further 8 weeks (Fig. 3f). The same trend is evident within the bone shaft (Supplementary Fig. 3). The retention of tungsten only in cortical bone is consistent with remodeling activity in these tissues since cancellous bone has significantly higher rates of remodeling compared to cortical bone[10]. Thus, while cancellous bone quickly accumulates tungsten, it is also the first tissue to replace tungsten impregnated tissue with new bone once the source is removed. By contrast, retention is observed within cortical bone, which suggests that this tissue may act as a reservoir and a source of chronic tungsten exposure even after the original source is removed.

Chemical speciation of tungsten in vivo. The potential toxicity of tungsten within bone tissue is likely influenced by its chemical form therein. Indeed, speciation-specific toxicity in aquatic organisms has been reported for mono- and polytungstate species[2]. To identify the local coordination structure of tungsten within bone samples, eight SR-µXANES measurements were
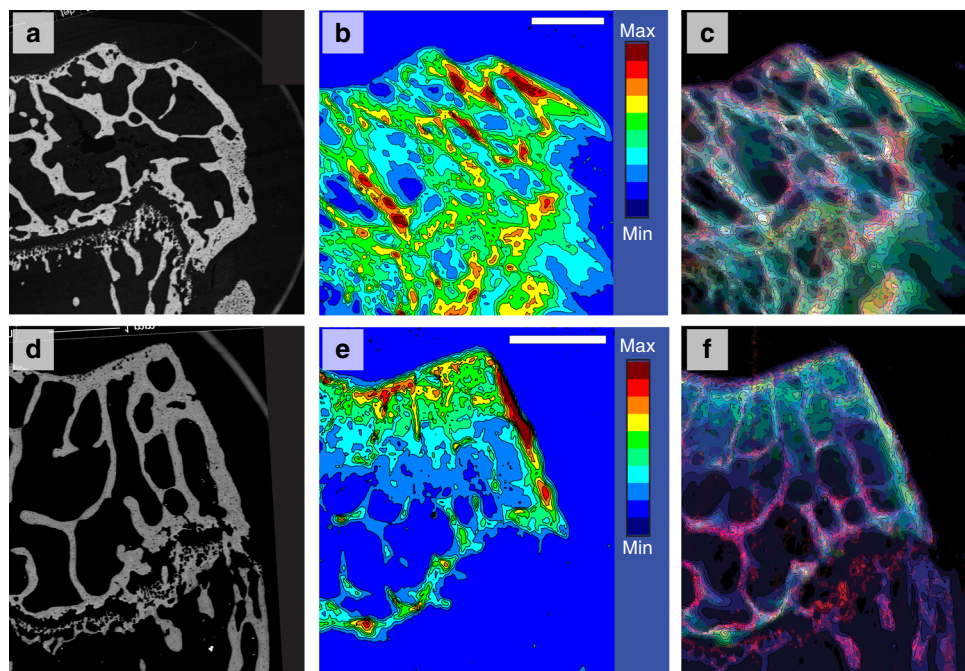
Fig. 3 Comparing element distribution in mouse femur head after tungsten source is removed. **a**–**c** Femur head of mouse exposed to 4 weeks of tungsten (1000 ppm). **d**–**f** Femur head of mouse exposed to 4 weeks of tungsten (1000 ppm) followed by 8 weeks of non-contaminated tap water. **a**, **d** BEI corresponding to SR-µXRF images. **b**, **e** Tungsten deposition map generated using SR-µXRF. Scale bars 500 µm. **c**, **f** Overlay images of calcium (red), tungsten (green), and zinc (blue) elements determined from SR-µXRF. See Supplementary Table 1 for intensity values
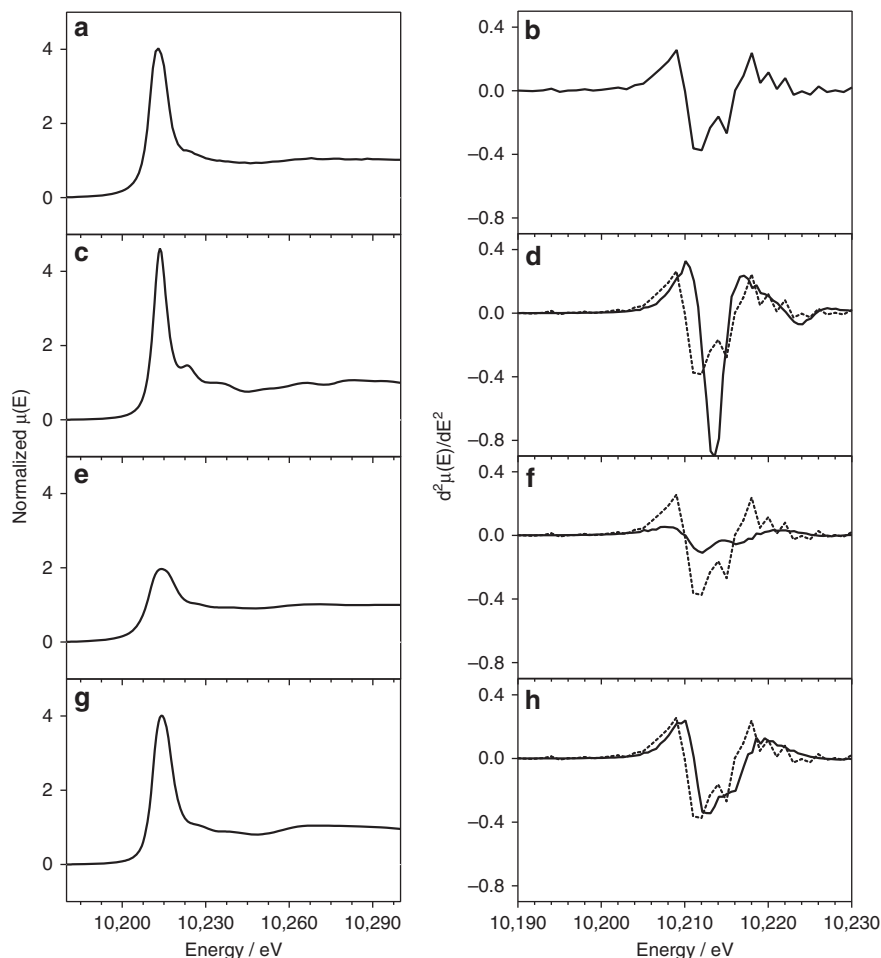
Fig. 4 Comparison of XANES spectra for tungsten in bone with tungsten standards. Averaged tungsten L3-edge μ-XANES spectra (a) with its second derivative (b) recorded for bone samples; XANES spectra of tungsten standards: sodium tungstate (**c**, **d**); ammonium paratungstate B (**e**, **f**); and phosphotungstate ($H_3PW_{12}O_{40}$) (**g**, **h**). To facilitate comparison, the spectrum in **b** is displayed as dashed lines in **d**, **f**, **g**

recorded across varying regions of cancellous and cortical tissues in tibia and femur samples (Supplementary Fig. 4). The essentially identical spectra obtained (Supplementary Fig. 5) are indicative of a remarkably consistent speciation profile and suggest that the chemical form of tungsten within this biological tissue is not influenced by environmental differences within bone physiology nor by the removal of the tungsten source following 4 weeks of exposure. The local concentration also does not appear to affect its speciation since spectra were recorded in areas displaying both high and low tungsten fluorescence intensity.

There are, however, marked differences between the averaged XANES spectrum of tungsten in bone samples and that recorded for the form in which was administered, namely sodium tungstate (Fig. 4a, c). This indicates that there is a change in tungsten speciation during uptake and/or deposition in bone tissue. A comparison of the second derivative of the XANES spectra more clearly highlights this difference (Fig. 4b, d) but, more importantly, provides structural information regarding the coordination geometry around tungsten and can be used to identify a specific species[11]. The two closely spaced 2nd derivative minima observed for the bone sample at 10.211 and 10.215 keV are not consistent with a tetrahedral geometry, which, as seen for sodium tungstate (Fig. 4d), produces a single sharp minimum. Instead, this feature is indicative of a tungstate species, which adopts a distorted octahedral geometry, similar to that observed in crystal structures of various polytungstates. The poor congruency between the spectra recorded for tungsten in bone

samples and that of paratungstate B ($H_2W_{12}O_{42}^{10-}$), however, indicates condensation of ingested sodium tungstate into this polytungstate form does not occur (Fig. 4e, f). By contrast, close agreement is observed with the heteropolytungstate, phosphotungstate ($H_3PW_{12}O_{40}$, Fig. 4g, h). This molecule consists of twelve oxo-bridged tungsten atoms that surround and share ligation of a phosphate anion in what is referred to as a Keggin structure[2]. The similarity of the phosphotungstate XANES spectrum to that measured for tungsten in the bone samples suggests that the majority of tungsten present within bone tissue exists in a similar local coordination environment. The low pH conditions and high phosphate concentrations present during the bone remodeling processes could certainly favor the formation of phosphotungstate within bone tissue[12], but the formation of additional tungstate species in minor quantities cannot be discounted. The low pH in gastric juice will favor polytungstate formation, but the ambient low concentrations of tungstate in the stomach is expected to limit polytungstate formation. This finding has important implications for tungsten toxicity since phosphotungstate is a well-established redox catalyst[2,13]. It is also a new mechanism for the in vivo toxification of a soluble metal with the other recognized mechanism being metal methylation[14].

Discussion

In summary, we present the novel finding of site-specific, heterogeneous tungsten accumulation attaining levels ~10-fold

greater than the background level. These levels are persistent, even once dietary exposure ceases. Furthermore, SR-µXANES studies indicate that tungsten in bone tissue is similar to the heteropolytungstate species phosphotungstate. This is alarming on a number of levels. Phosphotungstate is a known redox active catalyst, and thus, if formed during bone remodeling, may have numerous deleterious biochemistries affecting essential bone functions, including growth, structure and immune cell formation. As ongoing studies continue to implicate tungsten in a variety of medical conditions, including promoting tumorigenesis, it is a concern that the World Health Organization has no water regulations for tungsten[3,4]. The findings reported are essential for ongoing efforts to understand tungsten's effects on various biological processes and are crucial for the development of new, effective therapeutic methods for its mobilization and removal.

Note added in proof: During the production of this Article an important Review of tungsten implant weathering was published.[15]

Methods

In vivo tungsten exposure. Animal experiments were performed under a McGill University Animal Care Committee approved protocol. Four-week-old male C57BL/6 J mice were purchased from Charles Rivers Laboratories Inc. (Montréal, Québec) or bred in house and were given food and water ad libitum. After 1 week of acclimation, mice were divided into two treatment groups: control tap water or 1000 mg/L tungsten. Mice were exposed for 1, 4, or 12 weeks. An additional study compared removal of tungsten for 8 weeks, following a 4-week exposure to 1000 mg/L tungsten. For studies where mice were exposed to 1000 mg/L tungsten, the appropriate amount of sodium tungstate dihydrate ($Na_2WO_4 \cdot 2H_2O$; Sigma-Aldrich) was dissolved in tap water and was replaced every 2 or 3 days to limit conversion to polytungstates. As we have previously published[8], no changes in animal weight, physical appearance, or water intake were observed in the tungsten-exposed group.

Bone preparation for 4 week cross-sections. Mice were killed by CO_2 asphyxiation followed by cardiac puncture or cervical dislocation. Tibia and femur bones were removed, bone marrow was flushed and the samples were stored at −80 °C. To mount the samples, bones were cut in half, washed with 70%, 80%, 90%, 100% absolute alcohol followed by two washes with xylene and three washes of methyl methacrylate (MMA) before finally being set in MMA. 10 µm cross-sections cutting using a diamond blade and set on Kapton tape for SR-µXRF measurement.

Bone preparation for all other samples. Mice were killed by CO_2 asphyxiation followed by cardiac puncture or cervical dislocation. Tibia and femur bones were removed and the bones were placed for 1 week in a solution of 4% paraformaldehyde for fixation. Bones were then washed three times with a solution of 1% phosphate-buffered solution (PBS) at pH 7.4 and stored in the same solution. To mount the samples, bones were dehydrated using a series of alcohol washes followed by washes with xylene and MMA before finally being set in MMA. Using a diamond saw, samples were cut longitudinally before being polished using 600 grit silicon carbide paper and 6 and 1 µm diamond suspension. The surfaces were then carbon coated for backscattered electron imaging (BEI). Following measurement, thin sections of the samples were prepared by cutting with a diamond saw and further grinding down the back of the samples with 120 grit silicon carbide paper, leaving the surface untouched for SR-µXRF measurement. This preparation technique allowed for visualization of the surface using BEI, which was essential for comparing XRF maps to bone morphology. However, it also resulted in minute variations in sample thickness which made quantitative determinations of local concentration difficult due to difference in illuminated volume across the sample.

Backscattered electron imaging. Backscattered Electron Imaging experiments were done on a FEI Inspect F50 FE-SEM with EDAX Octane Super 60 mm² SDD and TEAM EDS Analysis System.

SR-µXRF and µXANES. SR-µXRF measurements in various modes were performed at two different synchrotron radiation facilities to study the (trace) elemental distribution in tibia and femur bone tissue. Control as well as 1- and 4-week tungsten-exposed samples were measured at the Canadian Light Source (CLS) in Saskatoon, Canada. Samples exposed to tungsten for 12 weeks continually and tungsten for 4 weeks followed by 8 weeks of tap water and were measured at the National Synchrotron Light Source II (NSLS-II) in Upton, USA. SR-µXRF experiments were carried out at the VESPERS beamline at CLS and at the 5ID beamline at NSLS-II. In vivo L_3-edge tungsten µ-XANES spectra were collected at

the SRX beamline, on bone samples at different eight locations (Supplementary Fig. 4). Owing to the observed congruency, all eight recorded spectra were merged using the Athena software package.

All SR-µXRF measurements on the VESPERS beamline at CLS were performed using the polychromatic incident beam ("pink beam" mode), which covered the energy from 5–30 keV and with a beam size of 3 µm. Samples were mounted on a motorized stage at 45° angle in respect to the incident X-ray beam. A 4-element silicon drift Vortex detector was used to collect the XRF spectra, which was placed in the horizontal polarization plane at 90° to the incident X-ray beam (and 45° to the sample) with a sample-to-detector distance of 50 mm. The SR-µXRF maps were generated from deadtime-corrected XRF spectra with normalization to the flux of incident X-ray beam measured by an ion chamber.

The sub-micron resolution X-ray spectroscopy (SRX) beamline, located at 5-ID of the NSLS-II, is fed by an in-vacuum undulator. The high-brightness white beam is incident upon a harmonic rejection mirror and then into a fixed-exit Si(111) double-crystal monochromator, both of which deflect the beam horizontally. The monochromatic X-ray beam passes through a secondary source plane (In the "high flux" mode, the harmonic rejection mirror is bent to produce a ~70 micron image of the primary source in this plane, while in the "high energy resolution" mode, the mirror is flattened and an aperture forms the secondary source in the horizontal direction. The current work was performed in the "high-flux" geometry.), which serves as the effective source for the final focusing optics, a Kirkpatrick–Baez mirror pair. These fixed-figure mirrors are designed to produce a slightly sub-micron X-ray spot on the sample. To collect an X-ray fluorescence map, the sample is scanned through this beam on a crossed pair of stages with a continuous travel range of 50 mm (H) × 40 mm (V) measured with a 5 nm encoder resolution. µ-XANES or EXAFS is accomplished by a coordinated motion of the undulator gap and the monochromator. The photon flux incident upon the sample is measured by an ion chamber, the fluorescence is measured by a 3-element silicon drift detector, and the transmitted flux may be measured on a diode behind the sample. All µ-XANES measurements were collected in fluorescence mode.

VESPERS and 5-ID beamlines each had their individual advantages and disadvantages, however, their different specifications ultimately meant we could not perform quantitative comparisons between the data generated (Supplementary Table 1). The polychromatic beam at VESPERS allowed the visualization of light elements such as calcium albeit with a lower detection limit. Tungsten specific incident energy and small spot size at 5-ID allowed higher limit of detection with a higher resolution and the ability to collect XANES spectra in situ.

XANES. X-ray absorption experiments on reference samples were carried out at beamline 17 C in the National Synchrotron Radiation Research Center (NSRRC), Hsinchu, Taiwan. BL17C is a wiggler beamline and photoflux is around 5×10^{10} at a 4 mm(H) × 2 mm(V) beam size. The sample was sealed in a cell with Mylar windows and the experimental beam size was 3 mm(H) × 2 mm(V). The background subtraction and normalization of the XAS data, according to $\chi(k) = [\mu(k) \times \mu_0(i)]/\Delta\mu_0(0)$, were done by the AUTOBK program[16], where $\mu(k)$ is the measured absorption coefficient, $\mu_0(k)$ is the background, and $\Delta\mu_0(0)$ is the edge jump. The wave number is defined as $k = [2\ m(E-E_0)/(h/2\pi)]^{1/2}$, in which E, E_0, $h/2\pi$ and m are the photon energy, threshold energy, Planck constant, and mass of the electron, respectively. For the XANES data analysis, the pre-edge peak is isolated from the normalized XAS spectrum.

Spectra were aligned using the Athena software package (v0.9.24) and second derivatives calculated using the GraphPad Prism (v6.07) software package. Energy calibration of all recorded spectra (samples and standards) was performed using a tungsten foil as the reference ($E_0 = 10,207$ eV) in the Athena software package.

Data processing. XRF data obtained from the NSLS-II were deconvoluted with the PyXRF software package (https://github.com/NSLS-II-HXN/PyXRF). XRF data obtained from CLS were subjected to the same analysis but were first converted into HDF5 format using an in-house python script. The data were normalized by incident beam count values and graphed in OriginPro 9. A histogram analysis was performed on the intensity data to determine upper and lower limits of SR-µXRF plots. These values were selected such as to exclude the bottom and top 0.05% of the outlying data.

Data availability. Computer codes used in processing data and data that support the findings of this study are available from the corresponding author upon request.

References

1. *Molybdenum and Tungsten Enzymes.* (eds Hille, R., Schulzke, C. & Kirk, M.L.) (Royal Society of Chemistry, 2016). https://doi.org/10.1039/9781782628828

2. Strigul, N. Does speciation matter for tungsten ecotoxicology? *Ecotoxicol. Environ. Saf.* **73**, 1099–1113 (2010).

3. Bolt, A. M. et al. Tungsten targets the tumor microenvironment to enhance breast cancer metastasis. *Toxicol. Sci.* **143**, 165–177 (2015).

4. Lemus, R. & Venezia, C. F. An update to the toxicological profile for water-soluble and sparingly soluble tungsten substances. *Crit. Rev. Toxicol.* **45**, 388–411 (2015).

5. Guandalini, G. S. et al. Tissue distribution of tungsten in mice following oral exposure to sodium tungstate. *Chem. Res. Toxicol.* **24**, 488–493 (2011).

6. Pemmer, B. et al. Spatial distribution of the trace elements zinc, strontium and lead in human bone tissue. *Bone* **57**, 184–193 (2013).

7. Bolt, A. M. et al. Tungsten promotes sex-specific adipogenesis in the bone by altering differentiation of bone marrow-resident mesenchymal stromal cells. *Toxicol. Sci. Toxicol. Sci.* **150**, 333–346 (2016).

8. Kelly, A. D. R. et al. In vivo tungsten exposure alters B-cell development and increases DNA damage in murine bone marrow. *Toxicol. Sci.* **131**, 434–446 (2013).

9. Gomez, S., Rizzo, R., Pozzi-Mucelli, M., Bonucci, E. & Vittur, F. Zinc mapping in bone tissues by histochemistry and synchrotron radiation–induced x-ray emission: correlation with the distribution of alkaline phosphatase. *Bone* **25**, 33–38 (1999).

10. Clarke, B. Normal bone anatomy and physiology. *Clin. J. Am. Soc. Nephrol.* **3** (Suppl 3), 1–12 (2008).

11. Hur, H. & Reeder, R. J. Tungstate sorption mechanisms on boehmite: Systematic uptake studies and X-ray absorption spectroscopy analysis. *J. Colloid Interface Sci.* **461**, 249–260 (2016).

12. Blair, H. C. How the osteoclast degrades bone. *Bioessays* **20**, 837–846 (1998).

13. Hill, C. L. in *Comprehensive Coordination Chemistry II* (eds McCleverty, J. A. & Meyer, T. J.) 679–759 (Elsevier Inc., New York, 2004).

14. Drobna, Z., Styblo, M. & Thomas, D. J. in *Current Protocols in Toxicology* (John Wiley & Sons, Inc., New York, 2009). https://doi.org/10.1002/0471140856. tx0431s42

15. Shah Idil, A. & Donaldson, N. The use of tungsten as a chronically implanted material. *J. Neural Eng.* in the press. https://doi.org/10.1088/1741-2552/aaa502.

16. Harrop, T. C., Song, D. & Lippard, S. J. Interaction of nitric oxide with tetrathiolato iron (ii) complexes: relevance to the reaction pathways of iron nitrosyls in sulfur-rich biological coordination. *Environments* **128**, 3528–3529 (2006).

Acknowledgements

Author contributions

Additional information

Supplementary information is available for this paper at https://doi.org/10.1038/s42004-017-0007-6.

Reprints and permission information is available online at http://npg.nature.com/reprintsandpermissions/

Publisher's note: Springer Nature remains neutral with regard to jurisdictional claims in published maps and institutional affiliations.